Failure and strengthening of granular slopes under horizontal vibration

Douglas Rubin, Naomi Goldenson, and Greg A. Voth

Department of Physics, Wesleyan University, Middletown, Connecticut 06459, USA

We present experimental measurements of a granular slope under horizontal vibration. We use optical particle tracking to measure the motion of surface beads as the slope fails. We find that for all but the largest inclination angles, initial bead motion leads to strengthening rather than an avalanche. The initial motion of the beads is usually intermittent and evolves differently for different preparations, slope angles, and rates of increase in the vibration amplitude. When a specific criterion is chosen to define failure, the Coulomb friction model adequately describes the average acceleration required to produce failure, as long as slope preparation and experimental protocol are constant. However, the observed intermittent motion and rate dependence indicate that strengthening microrearrangements are important features that affect failure of slopes under external perturbations.

I. INTRODUCTION

The failure and avalanching of granular slopes is important in many engineering and geophysical processes. The conceptual framework of an angle of repose, θ_r, and a larger maximum angle of stability, θ_m, with a metastable region between has been used effectively in describing many experiments using gradually inclined slopes and rotating drums [1,2]. The existence of the metastable region points to the significance of external perturbations in the failure of slopes. In the conceptual picture provided by the jamming phase diagram [3], perturbations can be thought of as similar to temperature in the way they allow a system to unjam.

A variety of perturbations applied to granular slopes including dropping individual beads [2,4] and vibration [5–7] have been studied. One of the early papers to provide experimental data questioning self-organized criticality was by Jaeger *et al.* [5], who looked at a vibrated rotating cylinder. They parametrized the effect of vibration by a decrease in the repose angle, and found that this depends on the logarithm of time. Tennakoon and Behringer [6] studied the failure of a granular bed under both horizontal and vertical vibration. King *et al.* [7] followed with a similar and more extensive study. Since a horizontally and vertically vibrated bed naturally forms heaps against one wall, both of these groups studied slope stability also. They found that the simple Coulomb model which uses a single friction coefficient to parametrize the strength of the material is quite successful in describing initial failure, although both experiments point out quantitative limitations of the model.

However, there are good reasons to expect that the simple Coulomb model should fail qualitatively in describing the failure of vibrated slopes. In the Coulomb model, the internal friction coefficient parametrizes many things including interparticle friction, particle shape, and the packing configuration. Since vibration causes the packing configuration to evolve with time [8,9], the friction coefficient characterizing a granular slope should also evolve with time [10]. This may not matter if the initial failure weakens the system so that it accelerates into an avalanche. However, many recent studies have shown that well before failure, a granular slope begins to change due to microrearrangements [11–15]. Under vibration, flat granular layers also experience rearrangements of

the force network, and these occur at vibration acceleration well below the acceleration of gravity [9,16].

In this paper we present measurements that connect the growing understanding of microrearrangements with earlier studies on the macroscopic failure of vibrated granular slopes [6,7]. By precise tracking of particles in the surface layer, we quantify the small motions that occur during the initial failure process. The acceleration required to produce failure fits the Coulomb model as found in previous work. However, the time evolution of the surface particle motion shows complex intermittent motion. In addition, the acceleration at failure depends on the rate at which the acceleration is increased. Both of these phenomena are interpreted as a result of microrearrangements which allow the material to explore stronger configurations.

II. EXPERIMENT AND ANALYSIS

A. Apparatus and procedure

A schematic of the experimental setup is shown in Fig. 1. We prepare a flat granular bed consisting of glass spheres with diameter $d = 1.13 \pm 0.06$ mm in a box of dimensions $190d$ long, $100d$ wide, and we consider a bed depth of $10d$. The bottom plane of the box is covered in sandpaper (50 grit) to provide a frictional base for the granular bed. The box is designed such that θ, the angle of its bottom plane with respect to the horizontal, is adjustable. It rests on an oil table from Ling Dynamics which allows for smooth horizontal
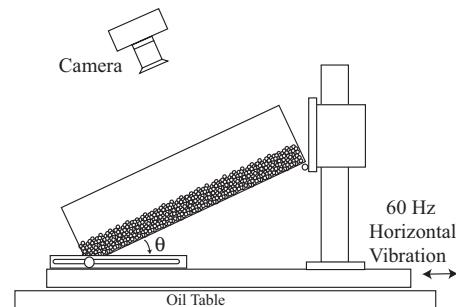

FIG. 1. A sideview schematic of the apparatus.

vibration. The table consists of a metal plate which rests upon a smooth granite surface, between which oil is continuously pumped to provide a low-friction environment. During the actual experiments, the oil pump is turned off so that none of the small vibrations that it induces may be transferred to the granular bed. The whole apparatus is constructed to allow the bed to be held rigidly at any angle so that internal mechanical modes of the structure are negligible compared to the applied acceleration.

To induce a surface avalanche, the box is sinusoidally vibrated in the horizontal direction by an electromagnetic shaker. The amplitude of the vibration acceleration increases linearly with time such that the amplitude of the acceleration at any time during an experiment can be expressed nondimensionally as $\Gamma(t) = tr(2\pi f)^2/g$, where t is the time since the start of the experiment, r is a constant of units m/s such that tr gives the displacement amplitude, f is the vibration frequency (60 Hz), and g is the acceleration due to gravity. For ease of notation we define $R \equiv r(2\pi f)^2/g$, which we call the "rate of acceleration ramping," so that $\Gamma = Rt$. The linear modulation was chosen to provide a smooth increase in acceleration so as to eventually perturb the granular slope into avalanche. We have also studied the effects of step increases in the acceleration and present some data using this method in Sec. IV. A piezoelectric accelerometer is used to measure the acceleration applied to the bed, and it is this measured acceleration that we use in subsequent data analysis.

To obtain surface particle velocities during the experiments, the surface of the granular layer is imaged with a digital camera positioned directly above it (Basler A504k, 1024×1280). We image an area of 3×4 cm^2 slightly above the center of the box, and capture approximately 800 particles in each frame. For each different θ that is used, the camera is adjusted so it is nearly perpendicular to the slope and then calibrated.

Camera images and box movement are synchronized allowing for a sensitive measurement of the particle velocities. That is, the image period is set to be an integer multiple of the shaking period, so that the box is in the same position every time an image is taken. The synchronization allows us to achieve a resolution in particle positions of ~ 0.05 pixels (1.5 μm). Converting to velocity yields a typical resolution limit of about 0.017 mm/s, although this changes from experiment to experiment given the utilized frame rate and pixel to length conversion.

We consider several experimental variables to study slope failure behavior: preparation procedure, inclination angle and the rate of acceleration ramping. Depending on the parameters used, the length of any experiment can range from about 10 s for large R and θ to about 10 min for small R and θ. For the shortest experiments images are acquired at 30 frames/s and for the longest, images are acquired at 6 frames/s due to the constraint of frame grabber memory.

It should be noted that we do not control the ambient humidity of the laboratory. Humidity can lead to the formation of cohesive liquid bridges between granular particles. However, we do not expect the bridges to significantly affect our large 1.13 mm spheres [17]. Moreover, changes in the pack strength of the material are not observed during the duration of any set of experiments which is at most a few days. We conclude that variation in environmental variables such as humidity does not significantly affect our results.

An experiment consists of first preparing the granular bed in the box; we compare two preparation methods. In method A the box is raised to a certain height, making all the beads bunch up at one end of the box. The shape and size of this bunched up formation is roughly constant, so that a consistent initial packing geometry and density can be achieved before leveling the bed. The box is repositioned to the horizontal, and a leveler is passed along the beads at a roughly constant velocity from the back of the box to the front so that a flat granular surface is produced. The leveler is then passed again from the front of the box to the back so that any extra beads above the flat surface will be at the bottom of the slope and therefore not susceptible to movement during vibration. The box is then slowly raised to the desired angle θ and secured. In method B the beads are prepared as in method A, but before being raised to θ, they are subject to a constant horizontal vibration of $\Gamma = 0.4$ lasting for 30 s.

After calibration and then preparation, the box is subject to acceleration at a specific rate of acceleration ramping, R, and images are taken throughout the whole failure process. We take images beginning before the onset of motion and continue until well after the surface remains continuously mobilized. Most experiments are completed before there is enough pileup of particles to create a significant decrease in the slope angle in the center of the chamber.

B. Data analysis

Particle positions and velocities are extracted from the image sequences using IDL particle-tracking software [20]. To improve velocity precision, we average individual particle velocities through consecutive images over a small time interval of 0.25 s. The averaging smooths small random fluctuations in particle velocity associated with uncertainties in the particle position measurements.

We quantify the evolution of surface particle motion by plotting the percent of surface particles that are mobilized and the mean surface particle velocity within our viewing window. We consider a particle mobilized if its velocity is above a threshold of 0.1 mm/s. This is more than five times the velocity resolution limit so will very rarely mistakenly identify a stationary particle as mobilized. Both profiles are plotted as a function of the amplitude of the applied acceleration Γ rather than time. This is equivalent to plotting versus time since for our linear acceleration ramping the amplitude is proportional to t.

C. Measuring the angles of repose and maximum stability

Our system's maximum angle of stability, θ_m, and angle of repose, θ_r, were determined experimentally for preparation method A by slowly tilting the box while imaging from the side. The slope angle was extracted by hand from the images both before and after each avalanche. The average angle at which the pile began to avalanche, θ_m, was found to be $24.2° \pm 0.5°$, and the average angle at which the avalanche halted, θ_r, was found to be $23.2° \pm 0.2°$. For comparison, Deboeuf *et al.* [4] utilized a similar method and found θ_m
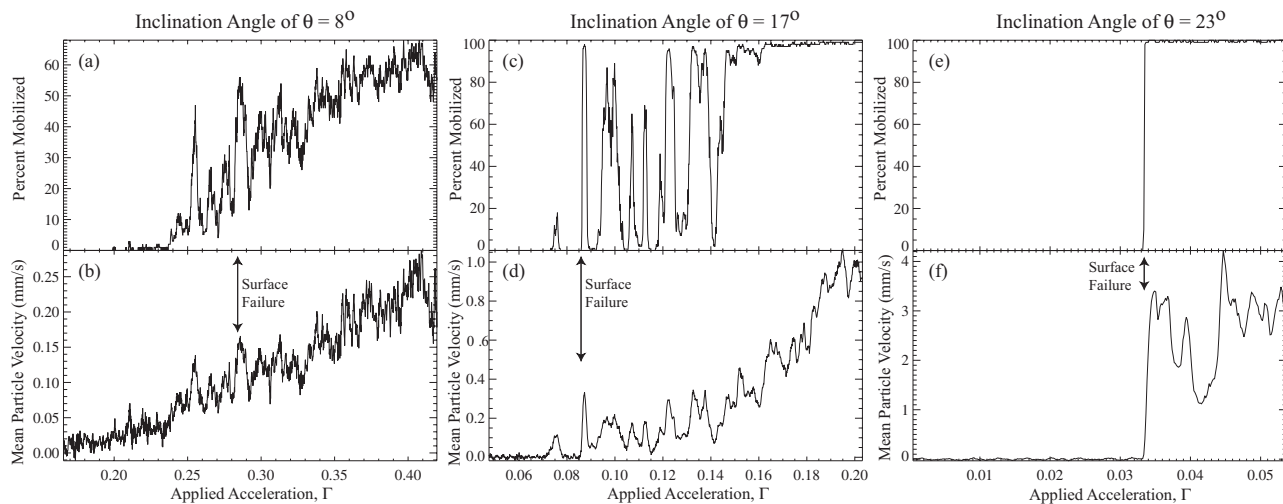
FIG. 2. Typical profiles of the percent of mobilized particles and mean surface velocity for three experiments with $\theta=8°$ (a), (b), 17° (c), (d), and 23° (e), (f). The upper row of plots (a), (c), (e) shows the percent mobilized and the lower row (b), (d), (f) shows the mean velocities. Arrows point to the acceleration that we define as surface failure: the first acceleration at which at least 50% of the surface particles are mobilized (see Sec. IV). Each experiment was prepared with preparation method A and performed with $R=0.003$ s^{-1}, a mid-range value of the acceleration ramping rates that we utilized. To visualize these failure processes, see the movies available at Refs. [18,19].

$=19.7°$ and $\theta_r=19.2°$ for steel beads in a rotating tumbler. On the other extreme, Daerr and Douady [2] found $\theta_m=32°$ and $\theta_r=26°$ for a slope of ten layers of much smaller glass beads. In general, for spherical particles, θ_r tends to vary between 19° and 26°, and θ_m between 20° and 32°, depending on the experiment. Various factors such as preparation, friction, container geometry, and cohesion can all affect these angles.

III. FAILURE MORPHOLOGY AT DIFFERENT INCLINATION ANGLES

The typical failure morphologies that appear at different inclination angles for preparation A are shown in Fig. 2. The three columns span angles ranged from $\theta=8°$ to 23°. The first row shows the percent of mobilized surface particles as a function of the amplitude of the vibration acceleration Γ, and the second row shows the mean velocity of all the particles at any given Γ. Movies of the failure process for these profiles (and for the profiles featured in the rest of this paper) are available [18,19].

Figures 2(a) and 2(b) show the mobilized percent and mean velocity, respectively, for one experiment with $\theta=8°$, the shallowest angle that we consider. At 8° the system is far below its angle of repose, and so gravitational load is weak. Hence, the fraction of beads that is mobilized and the mean velocity both increase relatively smoothly with the increasing acceleration as compared to the higher angle experiments [Figs. 2(c)–2(f)]. Here, a large vibration amplitude is required to induce significant surface mobilization and the particles gradually creep downhill.

At a steeper inclination angle of $\theta=17°$, shown in Figs. 2(c) and 2(d), the system's surface mobilization is intermittent. For this experiment, first a small fraction of the beads mobilize at $\Gamma=0.075$; then the layer stabilizes until $\Gamma=0.085$ when essentially all the beads mobilize, but again the

movement ceases. This intermittent behavior proceeds all the way to $\Gamma=0.145$ when finally the slope remains continuously mobilized, a regime which we will define as the "flow" regime and explore in detail in Sec. V B.

An important question is why the mobilization halts during the intermittent regime. Often the end of avalanching is interpreted by considering the decrease in slope angle that the particle motion has produced [5]. However, in almost all of our experiments, the change in slope angle after each transient failure event is too small to significantly stabilize the surface. In Figs. 2(c) and 2(d), note that even by $\Gamma=0.145$ the beads have only moved on average by about 4.5 bead diameters (less than 3% of the chamber length). This motion occurs over approximately seven small mobilization events so the average displacement in each event is about $0.6d$. A very rough model of the slope changes that result from this amount of movement gives an angle change of 0.03°. (Here we have assumed a parabolic velocity profile and that any beads that would leave the bottom of the chamber are distributed in a wedge over the lower half of the chamber, which gives $\Delta\theta=\frac{8}{3}\frac{hdx}{L^2}$ where dx is the particle displacement, h is the layer depth, and L is the chamber length.) We expect that this small angle change is negligible for restabilizing the slope.

Hence, alternative sources of strengthening are needed to account for the fact that the transients are able to halt against accelerations that were once able to produce failure. This strengthening after the initial mobilization of an inclined vibrated granular layer is one of the most robust results of our measurements. Interestingly, as will be addressed in Sec. V B, the intermittent dynamics vary considerably depending on the rate of acceleration ramping.

At $\theta=23°$ in Figs. 2(e) and 2(f), the system is nearly in the metastable region of $\theta=23.2°-24.2°$. A small perturbation in the form of vibration causes the highly inclined layer to mass avalanche, reaching a particle mobilization of about
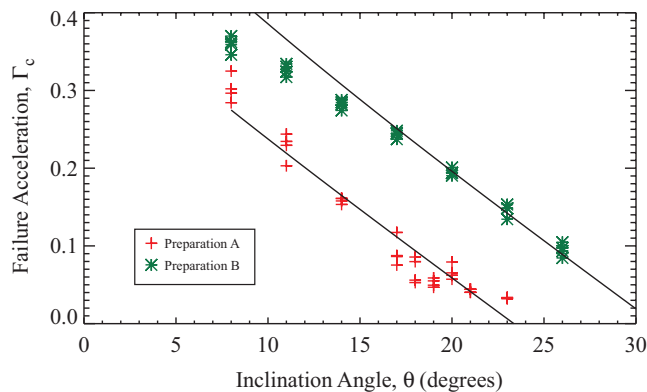
FIG. 3. (Color online) Surface failure accelerations across every inclination angle for both preparation methods. The solid lines are fits of the Coulomb model [Eq. (1)] with $\mu=0.43$ (preparation A) and $\mu=0.60$ (preparation B). ($R=0.003$ s^{-1}).

100% almost immediately at a modest $\Gamma=0.033$. Notice the decrease in mean velocity that occurs around $\Gamma=0.04$ after the initial failure in Fig. 2(f). We interpret this slowing as another case of the particle mobilization allowing the system to explore more resilient packing states. Here, though, the particle displacement before $\Gamma=0.04$ is about six bead diameters. This is less than 4% of the chamber length, but is estimated to produce an angle change of 0.3° which might partially account for the slowing.

IV. A COULOMB MODEL OF SURFACE FAILURE

To evaluate how the experimental parameters affect the failure process, we wish to identify the acceleration at which the vibrated slope fails. However, it is difficult to unambiguously identify the point of failure. The time evolution shown in Fig. 2 and the online movies [18,19] agrees with observations noted by King *et al.* [7], that surface rearrangements during the failure process such as chattering or localized avalanches preclude a rigorous identification of the failure point. We choose to define "surface failure" Γ_c as the first acceleration at which at least 50% of the surface particles are mobilized. Arrows in Fig. 2 indicate the location of Γ_c for these experiments.

Figure 3 shows the dependence of Γ_c on both inclination angle and preparation method, where each data point represents the failure of an individual experiment. As expected, the acceleration required to induce failure decreases to zero as the angle increases. For preparation A, Γ_c goes to zero near 23°, which is close to our measured maximum angle of stability of $\theta_m=24.2°$ from Sec. II C.

Preparation also influences the strength of our vibrated granular packs. Figure 3 shows that preparation B, with the applied horizontal vibration before the experiment starts, requires higher acceleration amplitudes to induce surface failure for every inclination angle. The added stability is a natural consequence of the known compaction of granular media under vibration [8], which leads to stronger packings.

Note also that there is much less variability in the failure acceleration for preparation B than for preparation A. Other

studies of the failure of slopes under vibration [6,7] have used vibrated preparation methods, presumably in part because of the reproducibility they provide. The particle tracking is sufficiently accurate that we are quite confident that the scatter in Fig. 3 represents variations in the failure process for different samples rather than experimental error. In any case, the small scatter in preparation B represents an upper bound on experimental error.

A first order model of failure for a horizontally vibrated slope follows from the Coulomb criterion [6,7] which states that relative slip motion between layers occurs when the tangential force on a layer, F_T, is equal to the frictional force μF_N, where μ is the coefficient of friction and F_N is the normal force. The model is derived from the forces associated with the vibration and gravity, which both contribute to the normal and tangential forces on the granular material. If failure is associated with the maximum acceleration during the sinusoidal vibration, then the horizontal acceleration amplitude required to produce failure at an angle θ is given by

$$\Gamma_c = \frac{\mu - \tan(\theta)}{\mu \tan(\theta) + 1}. \tag{1}$$

The model is plotted over the data in Fig. 3 for both preparations with $\mu=0.43$ for preparation A and $\mu=0.60$ for preparation B. The μ values were calculated from a nonlinear least squares fit of Eq. (1) to the data with μ as a free parameter. For preparation B, the least squares fit considered only the data above $\theta=15°$. The discrepancy between the data and the Coulomb model at these shallow angles might be related to the fact that the vibration amplitude used in preparing these systems is $\Gamma=0.4$, very close to where the data trend seems to intercept the y axis. This may be related to the observation by Umbanhower and van Hecke [9], that granular packs are resilient to perturbations up to the maximum perturbation they have previously received.

We can compare our results to those of King *et al.* [7] previously mentioned in Sec. I for the experiments where they considered zero-amplitude vertical acceleration. Under their definition of surface failure, they found that for glass spheres of diameter 180–300 μm, at $\theta=11°$ and 22°, their slope reached instability at $\Gamma \approx 0.5$ and 0.3, respectively. Our Γ_c values for these inclination angles are approximately half theirs. Many experimental differences between our study and theirs can account for our lower surface failure accelerations. The grains they used were smaller, possibly resulting in greater cohesive effects. The layer depth was significantly deeper (20–30 mm), requiring higher accelerations to induce fluidization as found by [10]. Other differences that might be important include preparation, vibration frequency, and the definition of surface failure.

V. STRENGTHENING

Our measurements show that a dominant feature of the failure of granular slopes under vibration is that they undergo strengthening. Losert *et al.* [21] provide a summary of many of the known strengthening mechanisms, while also introducing experimental investigations into shear induced
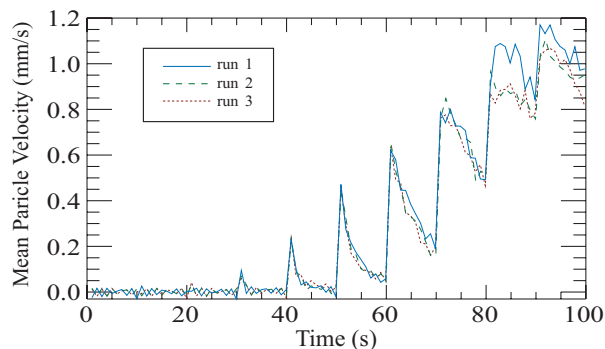
FIG. 4. (Color online) Three data sets showing the mean surface velocity with incremental increases in the acceleration. The inclination angle is 15°, and acceleration increments of $\Delta\Gamma = 0.06$ occur every 10 s. Note the decrease in velocity after each increment as the systems strengthens against the new, higher applied acceleration. The close agreement between the three runs attests to the reproducibility of the failure process of this system.

strengthening. External perturbations also induce strengthening, and previous work has identified several phenomena that might be important in our study including: microfailure rearrangements via the gravitational load of inclined systems [11,12] and the reinforcement of the force chain network under even extremely gentle vibration [9,16].

A. Strengthening due to discrete acceleration increments

The strengthening that occurs during the course of an experiment is most easily seen when the acceleration is ramped in discrete steps. Figure 4 shows the mean surface velocity as a function of time for three identical experiments in which the acceleration was incremented in steps. The data show large spikes in the mean velocity each time the acceleration is incremented, and each spike is followed by a rapid decrease in velocity. The induced motion allows the granular material to explore stronger configurations, and so the velocity decreases, sometimes going to zero. Again, we assert that the strengthening occurs as the mobilization allows the granular material to explore stronger packing configurations, since any decrease in slope angle is quite small. For example, between 50 and 60 s in Fig. 4, an average particle has moved at most only three times its diameter. During this time, though, a significant amount of strengthening has occurred, as the mean velocity has dropped by about 80%.

It should be noted that the preparation protocol used for these experiments differs slightly: the bed was leveled at the angle of interest rather than at the horizontal. However, our surface failure data indicate that this preparation method produces packs with strengths indistinguishable from the strengths of preparation A packs.

B. Strengthening due to continuous acceleration ramping

Strengthening is also observed when the acceleration is continuously increased as with the linear ramping. For example, the intermittent motion in Fig. 2(c) shows that the pack strengthens against the applied acceleration allowing
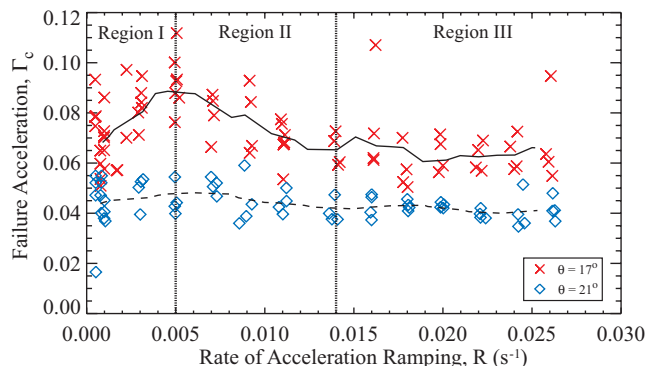

FIG. 5. (Color online) The dependence of the acceleration at surface failure on the rate of acceleration ramping, for two inclination angles $\theta = 17°$ and 21°. The 21° trend is fairly flat, whereas for the 17° data, three regimes are clearly apparent: $0 < R < 0.005$ s^{-1} where avalanche morphologies display transient strengthening events, $0.005 < R < 0.015$ s^{-1} where progressive pack strengthening is observed, and $R > 0.015$ s^{-1} which displays no strengthening. The scatter in this figure appears enhanced relative to Fig. 3 due to a smaller acceleration range in the y axis. The scatter at $R = 0.003$ s^{-1} is consistent, though, with the corresponding data in Fig. 3.

the transients to halt. We find that the amount of strengthening displayed by the slope is highly dependent on the rate at which the acceleration is ramped. To illustrate this dependence, Fig. 5 shows the acceleration required for surface failure, Γ_c, as a function of the rate of acceleration ramping, R. The crosses correspond to a midrange angle of $\theta = 17°$ and the diamonds correspond to $\theta = 21°$, an inclination just below the angle of repose. To guide the eye, we show curves smoothed over a small window of R.

In Fig. 5, three regions of strengthening with different slopes of the smoothed curve are apparent for $\theta = 17°$. At large R (region III) the acceleration required for failure remains constant, indicating that no significant strengthening has occurred. The $\theta = 21°$ data also show the same flat trend. The constant failure accelerations of $\Gamma_c = 0.065$ and 0.045 are thus a measure of the initial packing strength for $\theta = 17°$ and 21°, respectively. At $\theta = 17°$ and intermediate R (region II), the system progressively strengthens as the acceleration required for failure steadily increases with decreasing R. The region exhibits about a 30% increase in the acceleration required for surface failure. At the smallest R (region I), the failure acceleration decreases with decreasing R, indicating diminishing packing strength. Such behavior was quite unexpected and is a result of the distinctive failure morphology in the regime of small R which allows the definition of surface failure to be met early during the experiments.

The distinctive morphology is evident in Fig. 6, which shows the mobilized percent and mean velocity profiles for $\theta = 17°$ across the full range of the rates of acceleration ramping. For small R [Figs. 6(a) and 6(b)], transient many-particle mobilization events occur interspersed with periods when the slope is static. The first events occur at relatively small values of Γ, and the high mobilization ensures that they meet the definition of surface failure. As the events occur almost periodically, we were concerned that they might be an arti-
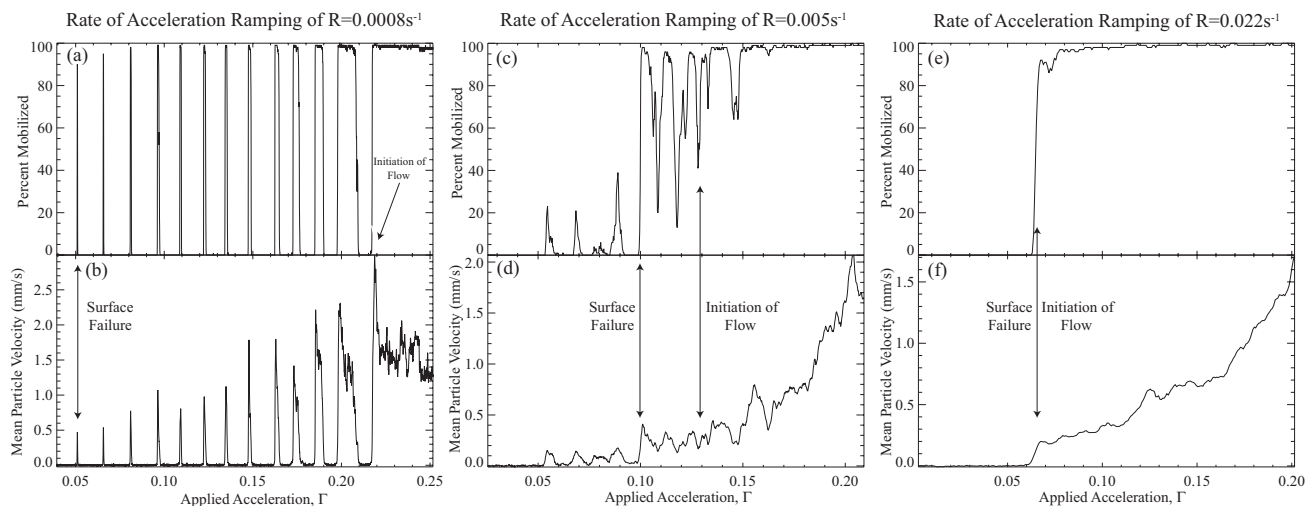
FIG. 6. Typical profiles of the failure process spanning the range of acceleration ramping rates, $R=0.0008$ (a), (b), 0.005 (c), (d) and 0.022 s^{-1} (e), (f). The upper row (a), (c), (e) of plots show the percent mobilized and the lower row (b), (d), (f) show the mean velocities. Arrows point to the acceleration at flow, the first acceleration where the percent of mobilized surface particles exceeds 50% and remains above 50% until the end of the experiment. Note the interesting avalanche morphology at $R=0.0008$ s^{-1} and its evolution with increasing R. These data sets use preparation method A and $\theta=17°$. To visualize these failure processes, see the movies available at [18,19].

fact of our procedure or equipment. There is no sign, though, of this periodicity in any of the acceleration measurements of the apparatus. Further, for different R, the difference in acceleration between events is nearly constant, and hence, the events cannot be the product of an external frequency. We conclude that at very low rates of acceleration ramping, these sequential failure events are characteristic of the failure process of vibrated granular slopes.

At larger R in Figs. 6(c) and 6(d), the initial events are of smaller magnitude, remaining below the 50% surface failure definition. By the largest values of R in Figs. 6(e) and 6(f), the behavior has completely subsided so that the failure process occurs with no initial transient features. This variation in avalanche morphology with the rate of acceleration ramping is a remarkable result of our study, suggesting rich internal packing evolution.

The strengthening behavior in regions II and III is fairly easy to understand. In region II, the small mobilization events before surface failure allow the system to explore more stable packing configurations. Moreover, since the acceleration increases slowly, the system has enough time to explore the configurations before the maximal force that a specific configuration can withstand is matched by the applied force. The contrary applies to region III as the acceleration increases rapidly enough so that critically high acceleration values are reached before the system can significantly strengthen. (As for the lack of observed strengthening in the $\theta=21°$ data, any mobilization events that could lead to strengthening result in immediate failure due to the high gravitational load.)

The puzzling behavior at very small R remains unexplained. It appears that there are microrearrangements that are below our detection threshold that reconfigure these packs so that the first measurable rearrangements span the entire system and so match our definition of failure. Presumably these microrearrangements occur at larger R also, but

only at very small R is there enough time for them to become important. Since the difference between small and intermediate R relates to whether the rearrangements span the system, we expect that the geometry and size of the system are likely to play a role in an explanation of the nearly periodic failure events at small R.

The lower values of Γ_c for small R result in a widening of the intermittent range. If we look at the upper end of the intermittent range rather than the first movement, we see a different behavior. We have been calling this regime where the particles are continuously mobilized the "flow" regime. We can rigorously define the onset of flow, Γ_f, as the first acceleration at which the mobilized percent of particles exceeds 50% and remains above 50% until the end of the experiment. Arrows in Fig. 6 point to the location of Γ_f for these experiments. To obtain an accurate measure of Γ_f, we purposefully extended the length of our experiments until the mobilization of the surface particles showed no obvious signs of decreasing.

Figure 7 shows Γ_f as a function of R for the same $\theta=17°$ and 21° data of Fig. 5. Utilizing this failure definition, progressive pack strengthening with decreasing R is observed for $\theta=17°$ all the way to $R=0$ s^{-1}. This failure definition reveals that the transients that occur at low R in region I are also effective in strengthening the pack since they further delay the onset of flow.

C. Strengthening of initially dense packs

The strengthening of slopes whose preparation included horizontal vibration (preparation B) is somewhat different than for the experiments without preliminary vibration (preparation A) that have been described above. Preparation B slopes usually exhibit a single initial peak in mobilization prior to the flow regime. Such failure morphology is seen across the whole spectrum of angles studied, as is shown by
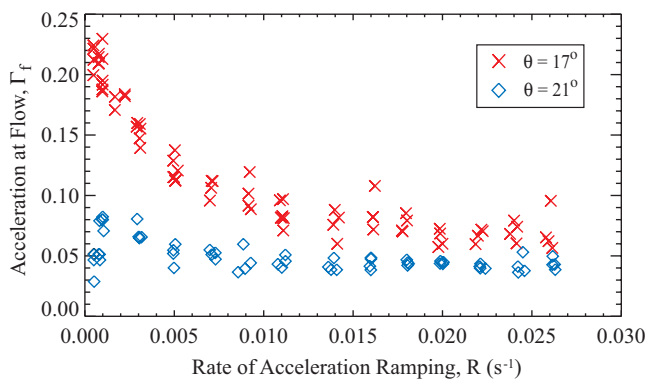
FIG. 7. (Color online) The dependence of the acceleration at flow on R for the same $\theta=17°$ and $21°$ data of Fig. 5. Under this definition, continuous pack strengthening is observed all the way down to $R=0$ s^{-1}.

FIG. 8. Avalanche profiles under preparation method B, the packs of higher density. Each experiment was performed with $R=0.003$ s^{-1}. (a), (c) The percent of mobilized surface particles during experiments for $\theta=8°$ and $23°$, respectively. (b), (d) The corresponding mean surface velocity profiles. The arrow in (c) points to the location of a small incipient peak sometimes observed before the main peak in the failure process for preparation B slopes. To visualize these failure processes, see the movies available at [18,19].

two typical experiments at extreme angles in Fig. 8.

We interpret the initial peak as a sudden reorganization of the force chain network as a result of the different directions of gravity between the preparation and the experiment. After preparation for both methods A and B, the weight of the particles is supported by force chains oriented vertically toward the bottom of the chamber. When inclined and vibrated, the force network fails, but is immediately replaced by a new network oriented to directly oppose gravity. In preparation A, this reorientation occurs gradually as the chains created in its preparation are relatively weak and easily reformed. But, for preparation B, the reorientation is much more dramatic as its dense initial packing results in strong chains which are less easily broken. Significant amplitudes of acceleration are therefore required to break the chains which produces the first peak in the mobilization. The chains then reform, creating a minimum in the mobilization, before the system finally begins to match the behavior of the other preparation.

This interpretation suggests connections with observations by Toiya *et al.* [22] in their study of granular shearing. They find that reversing the shear direction results in a transient during which the material is significantly weakened (analogous to our mobilization peak) until the anisotropic contact network reforms to resist the new shearing direction.

VI. CONCLUSIONS

Video imaging of the surface layer of a granular slope under external vibration provides a sensitive probe of the dynamics of granular packs as they fail. Our measurements have extended previous work on the effects of external perturbations on granular slopes by quantifying surface bead movements and exploring the time evolution of the surface motion. We find a wide variety of different failure morphologies depending on the inclination angle, preparation history,
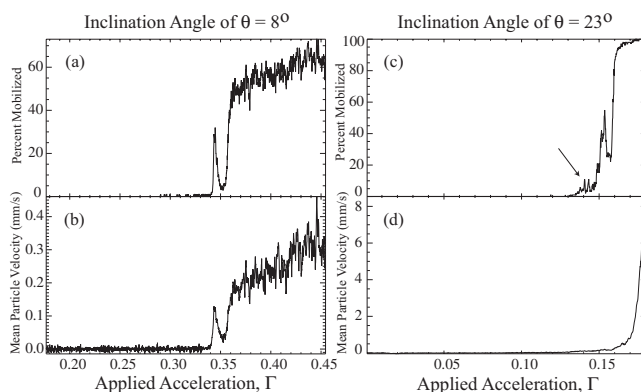
and the rate at which the vibration is increased. In agreement with previous work, we find that the Coulomb model is quite successful in modeling the acceleration required to produce surface failure. However, the time evolution of surface motion is more complicated than the Coulomb model predicts.

Possibly most interesting for future work on granular slopes is our demonstration of the importance of strengthening processes that restabilize granular slopes. These processes lead to intermittent failure and a dependence of the failure strength on the history of the perturbations on the system.

Our measurements suggest that perturbation induced compaction and fluidization of granular materials have much in common. In vibrated slopes, the rearrangements induced by the perturbation sometimes result in compaction and strengthening and sometimes lead to self-sustaining flows or avalanches. However, the rearrangements cannot be clearly separated into either strengthening microrearrangements or the complete failure of the slope. Instead, there are rearrangements across a broad range of scales each of which is initiated by the failure of a network and sometimes results in the formation of a new network capable of withstanding the perturbation.

[1] J. Duran, *Sands, Powders, and Grains* (Springer-Verlag, New York, 2000).

[2] A. Daerr and S. Douady, Nature (London) **399**, 241 (1999).

[3] A. J. Liu and S. R. Nagel, Nature (London) **396**, 21 (1998).

[4] S. Deboeuf, E. Bertin, E. Lajeunesse, and O. Dauchot, Eur. Phys. J. B **36**, 105 (2003).

[5] H. M. Jaeger, C. H. Liu, and S. R. Nagel, Phys. Rev. Lett. **62**, 40 (1989).

[6] S. G. K. Tennakoon and R. P. Behringer, Phys. Rev. Lett. **81**, 794 (1998).

[7] P. J. King, M. R. Swift, K. A. Benedict, and A. Routledge, Phys. Rev. E **62**, 6982 (2000).

[8] J. B. Knight, C. G. Fandrich, C. N. Lau, H. M. Jaeger, and S. R. Nagel, Phys. Rev. E **51**, 3957 (1995).

[9] P. Umbanhowar and M. van Hecke, Phys. Rev. E **72**, 030301(R) (2005).

[10] G. Metcalfe, S. G. K. Tenakoon, L. Kondic, D.-G. Schaeffer, and R.-P. Behringer, Phys. Rev. E **65**, 031302 (2002).

[11] A. Kabla, G. Debregeas, J.-M. di Meglio, and T. J. Senden, Europhys. Lett. **72**, 932 (2005).

[12] L. Staron, J.-P. Vilotte, and F. Radjai, Phys. Rev. Lett. **89**, 204302 (2002).

[13] L. Staron, J.-P. Vilotte, and F. Radjai, in *Powders and Grains 2005*, edited by R. Garcia-Rojo, H. Herrmann, and S. Mc-Namara (A. A. Balkema Publishers, London, 2005), Vol. 2, p. 831.

[14] S. Deboeuf, O. Dauchot, L. Staron, A. Mangeney, and J.-P. Vilotte, Phys. Rev. E **72**, 051305 (2005).

[15] O. Pouliquen and N. Renaut, J. Phys. II **36**, 923 (1996).

[16] A. Kabla and G. Debregeas, Phys. Rev. Lett. **92**, 035501 (2004).

[17] L. Bocquet, E. Charlaix, S. Ciliberto, and J. Crassous, Nature (London) **396**, 735 (1998).

[18] URL http://gvoth.web.wesleyan.edu/slopefailure/

[19] See EPAPS Document No. E-PLEEE8-74-164610 for movies of the failure process. For more information on EPAPS, see http://www.aip.org/pubservs/epaps.html.

[20] J. C. Crocker and D. G. Grier, J. Colloid Interface Sci. **179**, 298 (1996).

[21] W. Losert, J.-C. Geminard, S. Nasuno, and J. P. Gollub, Phys. Rev. E **61**, 4060 (2000).

[22] M. Toiya, J. Stambaugh, and W. Losert, Phys. Rev. Lett. **93**, 088001 (2004).